Measurements of permafrost thermal conductivity through CT-scan analysis

Marc-André Ducharme, Michel Allard, Jean Côté &
Emmanuel L'Hérault
Université Laval, Centre d'études nordiques, Québec, Québec, Canada

GEOQuébec 2015
Challenges from North to South
Des défis du Nord au Sud

ABSTRACT
When building in the Arctic, design considerations require precise knowledge of the thermal and geotechnical properties of permafrost. Computed tomography provides visualization of the cryostructure of permafrost. Previous studies showed great potential in using this technology for classification and volume measurements of permafrost components, i.e. sediment (solid), ice and gas (void) contents. The aims of this study are (1) to develop an innovative and non-destructive approach using a CT-scan to compute the thermal conductivity of undisturbed permafrost samples and (2) to validate the results computed from the CT-scan image analysis with proven experimental thermal conductivity data. Results obtained so far show that CT-scan thermal conductivity measurements yield results comparable to other existing methods. This new approach could still be significantly improved by the use of a higher resolution CT-scanner.

RÉSUMÉ
La construction dans l'Arctique nécessite une connaissance précise des propriétés thermiques et géotechniques du pergélisol. La connaisance de ces propriétés est également nécessaire pour le paramétrage des modèles de transfert de chaleur. Des études antérieures ont démontré le grand potentiel de l'utilisation de la tomodensitométrie pour les mesures du volume des composantes du pergélisol et la visualisation de la cryostructure. Une nouvelle approche est proposée pour mesurer la conductivité thermique du pergélisol. Les objectifs généraux de ce projet sont (1) d'élaborer une nouvelle méthode de caractérisation du pergélisol à l'aide de la tomodensitométrie et de modèle éprouvés et (2) de comparer et mettre au point une méthode novatrice pour mesurer la conductivité thermique et des paramètres géotechniques. Les résultats démontrent que les tests effectués à l'aide de la tomodensitométrie sont d'une valeur scientifique comparable aux données déjà existantes de conductivité thermique du pergélisol.

1 INTRODUCTION

Permafrost occurs in all types of geological surface material and contains ice in various forms and amounts. In order to prevent thaw settlement and drainage problems, precise knowledge of the thermal and geotechnical properties of the permafrost is needed. These property values are often used as input parameters in numerical modelling to assess the dynamic behavior of physical systems in both fundamental science and engineering. Although permafrost properties are rather well understood, new assays to measure them can yield insights into factors that define concepts such as thermal conductivity. These factors include ice content, soil grain-size and the structural organisation of ice within the soil. The aims of this study are (1) to develop an innovative and non-destructive approach to compute the thermal conductivity of undisturbed permafrost samples using CT-scan and (2) to validate the computed results with proven thermal conductivity data obtained on undisturbed permafrost samples.

2 METHODS

Nineteen undisturbed permafrost samples were chosen from different villages of Nunavik (Kangirsuk, Tasiujaq, Salluit) and Nunavut (Iqaluit, Clyde River and Hall Peninsula) to cover a large variety of cold regions soils. (Figure 1)

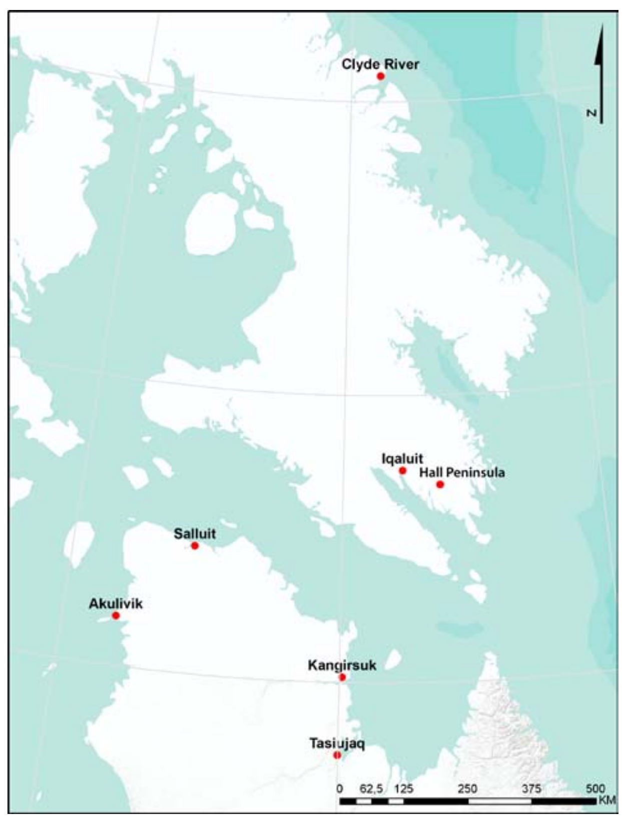

Figure 1: The various locations of the samples tested from Nunavik and Nunavut.

The cores were extracted from various sedimentary environments (glacial, alluvial, marine, organic, etc.), with different textures and cryostructures (ice and soil structural arrangement) ranging from homogeneous fine grained soils with stratified ice lenses to coarse-grained diamictons well-bonded with pore ice.

All samples were cored using a portable earth drill equipped with a core barrel (Calmels *et al*., 2005). This equipment allows a 100 mm diameter core to be retrieved almost unaltered. Cores were cut in a cold room using a concrete saw (Figure 2) to obtain samples with length ranging from 8 to 8.5 cm.

Figure 2: A) Permafrost cores are cut with a concrete saw at a temperature of -18°C B) Final dimensions of a sample.

2.1 CT-scan data

The permafrost samples were scanned using a Siemens Somatom 64TM scanner (Figure 3) at the Institut National de la Recherche Scientifique (INRS) in Québec city. Given the core diameter (100 mm) and scanner specification, a voxel resolution of 0.2 x 0.2 x 0.6 mm was obtained.

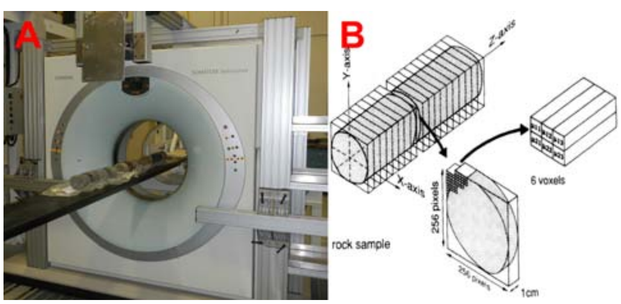

Figure 3: A) Sample scanning. The acquisition speed is very fast (a few seconds), thus the solid frozen state of permafrost is preserved. B) Principle of DICOM files and voxel; taken from Jacobs *et al.,* 1994.

Analysis of the cryostructure (Figure 4) was done using ORS Visual ™ software. This initial treatment aims to quickly visualize the permafrost internal cryostructure and summarily isolate tomographic intensity of permafrost components values.

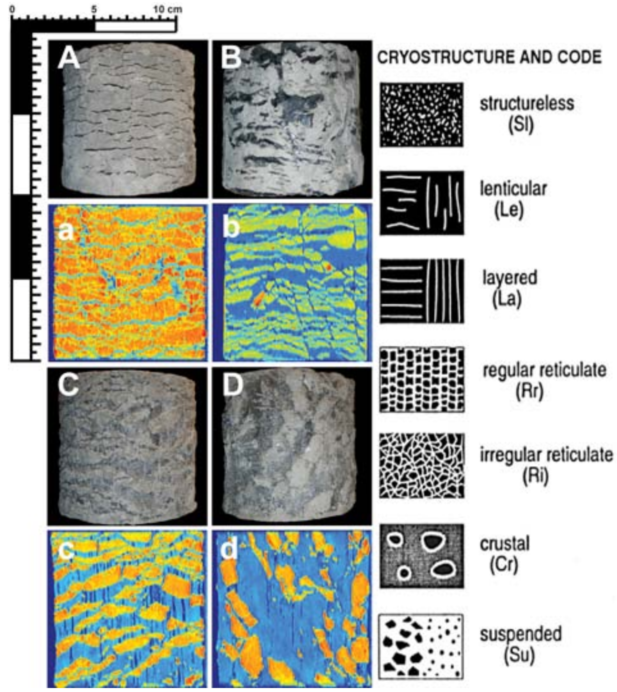

Figure 4: The classification of voxels by the script allows volumetric measurements of the three main components of permafrost: ice (blue), sediments (yellow to orange), ice and sediments (yellowish green) and gas (black). Examples of the wide range of cryostructure types based on the classification proposed by Murton and French (1994): A) layered/reticulate B) lenticular/irregular reticulate C) irregular reticulate D) suspended.

Previous studies from Jiang *et al.,* (2007) and Calmels *et al.,* (2010) measured the different ranges of tomographic intensity (CT number) (Table 1) that can occur in a permafrost sample. These values were used in a MatLab ™ script described in the work of Clavano *et al.,* (2011).

Table 1: Estimated CT number values of different permafrost materials according to Clavano et al., 2011 (taken from Jiang et al., 2007)

Material	Density (g/cm^3)	CT number (HU)
Air	0.000	-1000
Water	1.000	0
Ice	0.830 to 0.917	-170 to -83
Soil	0.880 to 2.000	-120 to 1920
Sand	1.442 to 2.082	844 to 2124
Clay	1.073 to 1.826	106 to 1612
Gravel, wet	2.002	1964
Stone	2.512	2984
Quartz	1.201 to 2.643	362 to 3246
Mica	1.602 to 2.883	1164 to 3726
Peat, dry	0.400	-600
Peat, moist	0.817	-183
Peat, wet	1.121	202

The script was developed by the research team at the Centre d'études nordiques with the consent and cooperation of the authors. It is designed to automatically discretize permafrost components (Figure 4) and perform highly accurate volumetric measurements. For each samples, the volumetric content of the frozen sediment and bubbly ice (x_{soil}, x_{bi}) was measured.

2.2 Thermal conductivity model

The calculation and measurement results were the central parameters used for modeling. The proposed model uses three general factors: 1) the soil type or texture (gravel and coarse sand, silt and clay, peat); 2) the porosity of the ice; 3) the cryostructure. The model also assumes that the permafrost consists of two separate main components:

frozen soil (x_{soil}, k_{soil})
bubbly ice (x_{bi}, k_{bi})

where x_{soil} and x_{bi} are the volume fractions of frozen soil and bubbly ice, and k_{soil} and k_{bi} are the thermal conductivities of the frozen soil and the bubbly ice, respectively. Therefore, the effective conductivity of a specimen is function of:

$$k_{eff} = fct(x_{soil}, k_{soil}, x_{bi}, k_{bi}) \qquad [1]$$

where thermal conductivity values (k_{soil}) are derived from known values from Côté and Konrad (2005) and volume fractions (x_{soil}, x_{bi}) are measured with CT-scan voxel classification.

The combined effects of the volumetric ratio and the cryostructure of a sample are computed by selecting a theoretical heat flow model depending on structural organization of the sample determined by visual analysis. The k_{eff} components have been used in three simple heat exchange models proposed by Farouki (1981):

$$k_{eff} = x_{soil}\ k_{soil} + x_{bi}\ k_{bi} \qquad \text{arithmetic mean} \qquad [2]$$

$$1/k_{eff} = x_{soil}/k_{soil} + x_{bi}\ /k_{bi} \qquad \text{harmonic mean} \qquad [3]$$

$$k_{eff} = (k_{soil})\hat{}(x_{soil})*(k_{bi})\hat{}(x_{bi}) \qquad \text{geometric mean} \qquad [4]$$

where the parallel flow model (vertical cryostructure) follows equation 2, the series flow model (lenticular and reticulate cryostructure) equation 3 and the geometric flow model (porous and suspended cryostructure) equation 4.

The general model used to compute the thermal conductivity of frozen soil (k_{soil}) is explained in Côté and Konrad (2005) (Figure 5):

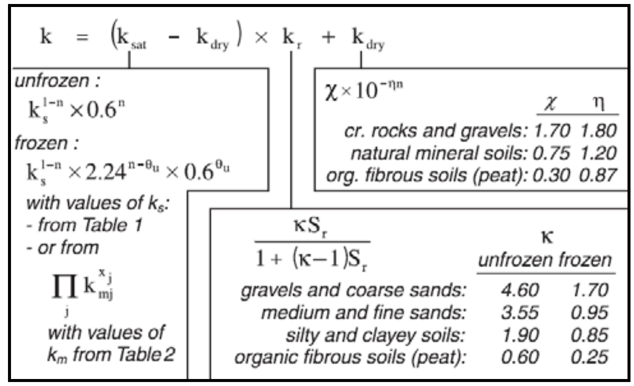

Figure 5: General thermal conductivity model from Côté and Konrad (2005)

The main equation in Figure 5 considers three general conditions: the saturated frozen soil thermal conductivity (k_{sat}), the dry soil thermal conductivity (k_{dry}) and the soil type (k_r). The k_{dry} parameter was calculated using the concept of structure effects on the thermal conductivity of a two-phase (fluid and solid) porous geomaterial (Côté and Konrad, 2009):

$$k_{dry} = (k_{2P}\ k_s - k_a)(1-nu) + k_a/1 + (k_{2P}-1)(1-nu) \qquad [5]$$

where k_{2p} is a structural parameter based on the pores connectivity factor (β), k_s is the thermal conductivity of solid particles, k_a is the thermal conductivity of fluid (air) and nu is the unfrozen soil porosity.

The thermal conductivity of the bubbly ice (k_{bi}) was found using an equation derived from Maxwell (1892) and proposed by Shwerdfeger (1963) to compute the thermal conductivity of sea ice:

$$k_{bi} = (2k_i + k_a - 2v(k_i - k_a))/(2k_i + k_a + v(k_i - k_a))*k_i \qquad [6]$$

considering the volumetric ratio of thermal conductivity of the air (k_a) and the thermal conductivity of the ice (k_i). The porosity of the ice (v) was estimated using HU (Hounsfield Unit) values (during the CT-scan analysis) of the ice contained in the sample using a statistical approach developed by Long et al., (2012):

$$v_{CT} = 1-(HU_{mean}+1024)/(HU_{max}+1024) \qquad [7]$$

where HU_{mean} and HU_{max} are the mean and maximum values for permafrost ice. The HU parameters were found during CT-scan analysis using values from Table 1.

3 RESULTS

Gravimetric ice content measurements were done to validate the volumetric measurements from the CT-scan. In order to compare volumetric and gravimetric ice content, the masses of melted water samples were transformed into ice volume (Figure 6). A strong correlation has been established between the actual fraction of ice (laboratory) and the volumetric ice fraction obtained from CT-scan data as shown in Figure 6.

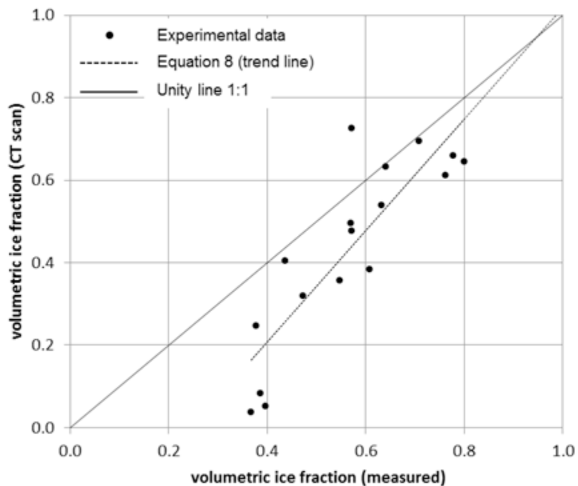

Figure 6: The strong linear relationship (R^2 = 0.74) between the volumetric ice fraction measured in laboratory and the CT-scan volumetric ice fraction.

The results demonstrate that the CT-scan tends to underestimate the volume of ice, since the volume of ice measured in the laboratory is considered the actual value. This was attributed to the size of the voxels usually exceeding the size of fine grained materials pores resulting in the CT-scan underestimating pore ice content. Thus, we can assume that there is a direct correlation between a porous and interstitial cryostructure and the increase of error.

The trend line found in Figure 6 was used as a calibration between volumetric ice fraction and CT-scan ice fraction that can be expressed as:

$$x_{bi}^{*} = 1.35x_{biCT} - 0.332 \qquad [8]$$

where x_{bi}^{*} is the corrected volumetric ice fraction and x_{biCT} is the CT-scan value for the volumetric ice fraction.

The ice content prediction found with equation 8 shows excellent results (Figure 7) when ice content is expressed in terms of gravimetric value (R^2 = 0.96).

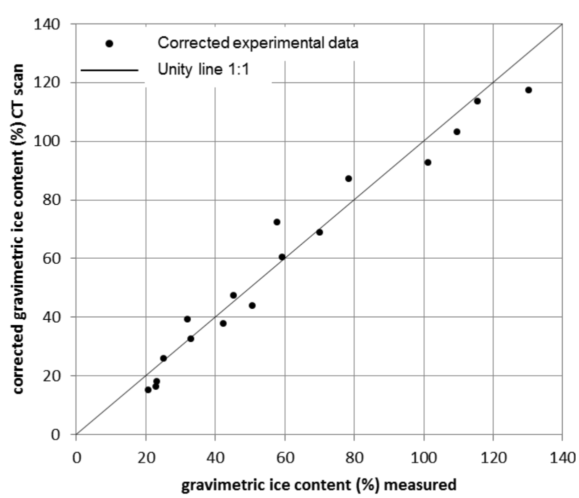

Figure 7: Calibration curve results for gravimetric ice content (%).

Considering equation 6, it was essential to establish the porosity of the ice within the permafrost samples. During the volumetric analysis of CT-scan images, the maximum and the average HU were measured and then integrated into equation 7 thereby obtaining an accurate estimate of the porosity of the ice. Table 2 demonstrates the close relationship between the ice content, the porosity of the ice, the thermal conductivities and the cryostructure of the samples.

Table 2: Results of gravimetric ice content, ice porosity, effective thermal conductivities and cryostructure.

Sample	Ice content (%)	Ice porosity (v)	Thermal conductivity (W/m°C)	Cryostructure
K11	22.80	0.18	2.28	Porous
K7	23.03	0.14	2.21	Porous
K6	20.68	0.14	2.16	Porous
K13	45.32	0.16	2.11	Porous/crustal
K3	32.02	0.14	2.10	Porous
K14	42.30	0.15	2.08	Porous/crustal
K16	33.05	0.16	2.04	Crustal (marine shells)
K17	57.72	0.16	1.94	Irregular reticulate
K9	50.65	0.18	1.93	Irregular reticulate
K5	59,26	0.16	1.92	Irregular reticulate
K8	25.16	0.18	1.89	Lenticular
K15	NA	0.12	1.86	Glacier ice
K12	115,47	0.16	1.84	Lenticular (0,5 – 1 cm ice lenses)
K18	109.52	0.16	1.83	Suspended
K2	101.13	0.18	1.79	Suspended
K4	78.34	0.18	1.76	Lenticular (0,5 – 1 cm ice lenses)
K10	70.12	0.21	1.70	Lenticular (1 – 2 cm ice lenses)
K24	751.38	0.20	1.57	Lenticular (1 – 2 cm ice lenses), peat
K19	130.22	0.27	1.51	Suspended

The suspended, lenticular and porous cryostructures have an average ice porosity of 0.20, 0.18 and 0.15. The high porosity of segregation ice, especially in the suspended and the well-developed lenticular cryostructures, are explained by the significant presence of bubbles trains (Figure 8).

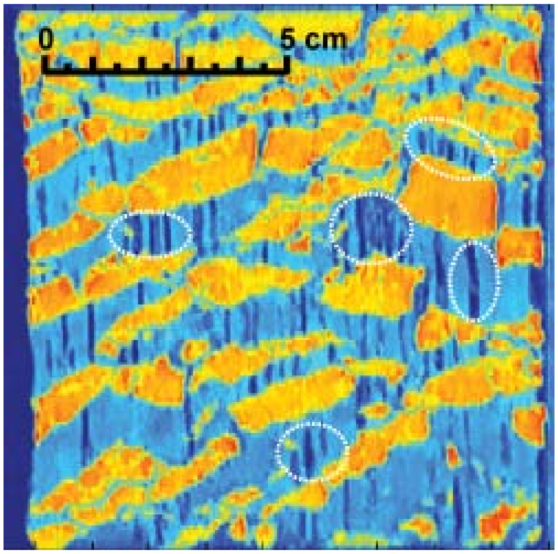

Figure 8: Gas concentration in bubble trains in sample K10.

The validity of the k_{bi} parameter (equation 6 and 7) was supported with the K15 sample (Figure 9). This buried glacier ice sample (interpreted as such according to the local stratigraphic context) from Iqaluit was the reference point setting because it shares characteristics with permafrost segregation ice.

Figure 9: Glacier ice sample (K15).

The computed result of thermal conductivity of the glacier ice, using equation 6, is 1.86 W/m°C. This rather low value is explained by the air content (v) of 12%. The effect of air bubbles on the thermal conductivity of ice was described in Schwerdtfeger (1963) and in Slusarchuk and Watson (1975). Many gaseous structures can be localized depending on the ice thickness (Calmels and Allard, 2004). Gas concentrations, or bubbles, are more abundant in thicker ice (suspended cryostructure and 1-2 cm ice lenses) layers and a gaseous coating is more apparent in thinner ice (0.5-1 cm ice lenses).

4 DISCUSSION

The numerous advantages and breakthroughs offered by the CT-scan become apparent when calculating volumes of permafrost components. The CT-scan can detect massive ice structures from frozen soil (suspended and developed lenticular) and gives excellent prediction of ice content. As shown in Figure 6 and Table 2, the CT-scan tends to under estimate volumetric ice fractions. This is especially true for very low ice fraction samples which mostly develop a massive interstitial cryostructure. The ice in this type of cryostructure is rather difficult to isolate in the CT-scan analysis given that pores in the soil matrix may be much smaller that the CT-scan resolution. However, the underestimation can be significantly reduced using the calibration (equation 8) proposed in this research. The linear regression could be used for future permafrost analysis using a similar resolution and type of CT-scan.

The thermal conductivity of pure ice is 2.24 W/m°C. As shown in Table 2, samples with high ice content do not approach this theoretical value in any case. The high porosity of the ice within samples with lenticular and suspended cryostructures (Figure 8) would explain this discrepancy. Often, the ice within epigenetic permafrost contains a great amount of gas concentrations. Thus, considering the air thermal conductivity (0.03 W/m°C) included in the ice, it is logical to find such a low thermal conductivity.

Our results obtained from the CT-scan compare well (Figure 10) with results obtained on similar permafrost soils by Slusarchuk and Watson (1975) on undisturbed ice-rich permafrost tested with a needle probe. Indeed, the particle size characteristics of the samples used in their study are very similar to those obtained during our geotechnical analysis i,e, 9% sand, 55% silt and 36% clay. These authors' results and ours show that the thermal conductivity of permafrost is strongly correlated with the gravimetric ice content of the permafrost. Samples with gravimetric ice content between 25% and 80% have an effective thermal conductivity from 1.81 to 2.12 W/m°C, whereas samples having ice contents ranging from 95% to 231% show thermal conductivities between 1.57 to 1.75 W/m°C. In general, the data show a decrease of the thermal conductivity as the ice content increases.

Leblanc (2013) measured thermal conductivity using *in situ* TDR probes specifically designed for permafrost soils (Slusarchuk and Foulger, 1973). Leblanc's tests were conducted in Salluit, on the same material (clay and silt) as samples K2, K9, K10, K18 and K19 with thermal conductivities values ranging from 1.5 to 2.2 W/m°C. The outcomes of the present study agree with Leblanc's conclusion that the frozen thermal conductivity is

controlled by the degree of saturation, which plays a key role on the formation of ground ice *i.e* the cryostructure.

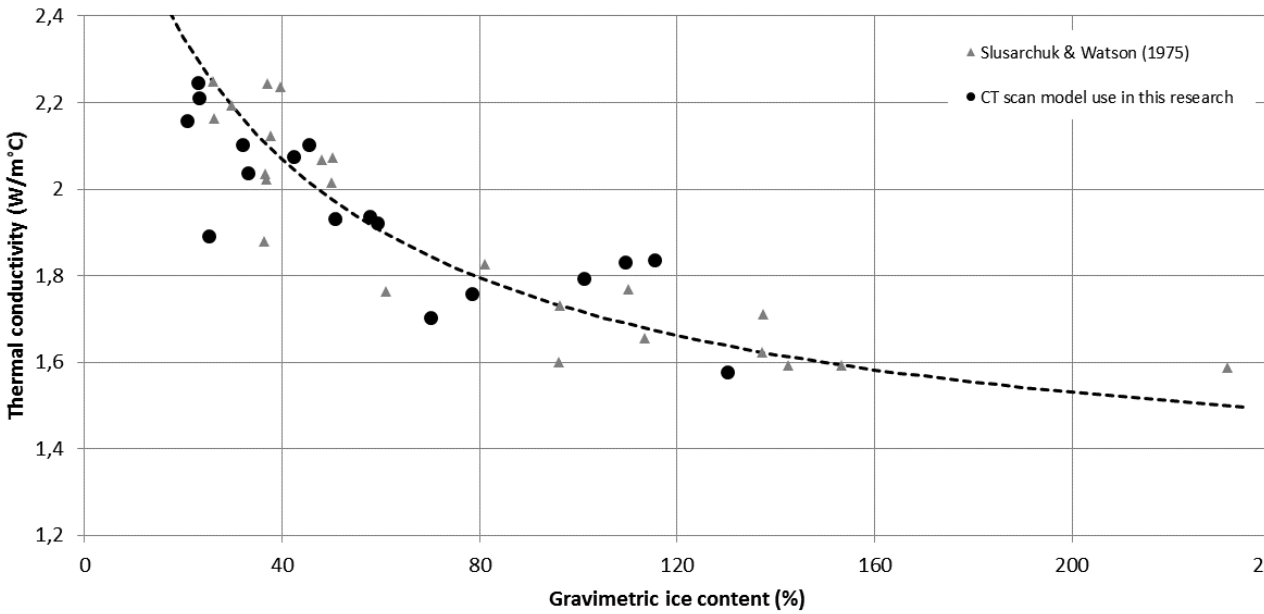

Figure 10: Our results demonstrated an excellent relationship with the thermal conductivity test (needle probe) data done on undisturbed ice-rich permafrost samples. When compared with a best fit curve derived on comparable samples from the data of Slusarchuk and Watson, the R2 is 0.8.

5 CONCLUSION

This research introduces an innovative approach to estimate the thermal conductivity of undisturbed permafrost samples. The development of the thermal conductivity model is based on the volumetric measurements provided by the CT-scan. The method was calibrated to take into account the interstitial ice fraction that cannot be precisely detected using the CT-scan at the available resolution. Adopting this calibration, the model and the image analysis provided realistic estimates of the thermal conductivity of permafrost ice. Thermal conductivity estimations take into account the porosity of ice, i.e. the presence of air bubbles. The new method (CT-scan/model) is a non-destructive approach that can be used to prepare and design permafrost-oriented engineering works for buildings and infrastructures.

Improvement could be done by using an apparatus with a higher image resolution, or establishing a better quantification and classification of voxels composed of ice/air and ice/sediment. The script could then be reviewed and enhanced with an improved voxel classification sheme to better discern the permafrost phases.

ACKNOWLEDGEMENTS

This research was supported by a number of individuals. The majority of the samples studied were provided from a former field campaign, thus reducing the logistical work. We thank Valérie Mathon-Dufour and Julie Leblanc-Dumas from CEN and Fabrice Calmels from Yukon College for their previous field works. Olivier Lachance and Étienne Hébert from Université Laval provided useful thermal conductivity raw data. Bernard Long and Louis-Frédéric Daigle from INRS operated the CT-scan and preprocess CT-scan images. Andrée-Sylvie Carbonneau from CEN refined the MatLab™ script. We are also thankful to the Inuit communities of Nunavik and Nunavut for their generous hospitability.

REFERENCES

Calmels, F. and Allard, M. 2004. Ice segragation and gas distribution in permafrost using tomodensitometry analysis. Permafrost and Periglacial Processes 15: 367 – 378.

Calmels, F., Gagnon, O. and Allard, M. 2005. A portable earth-drill system for permafrost studies. Permafrost and Periglacial Processes, 16: 311-315.

Calmels, F., Clavano, W.R. and Froese, D.G. 2010, Progress on X-ray computed tomography (CT) scanning in permafrost studies, GEO2010: 63rd Canadian Geotechnical Conference & 6th Canadian Permafrost Conference, Canadian Geotechnical Society: Richmond, B.C. 1363 – 1368.

Clavano, W.R., Calmels, F. and Froese, D.G. 2011, Quantitative processing of X-ray CT images of permafrost cores for cryostratigraphy : limitations and prospects, Submitted to Permafrost and Periglacial Procesesses (in review), 35 p.

Côté,J. and Konrad, J.M. 2005. A generalized thermal conductivity model for soils and construction materials, Can, Geotech, J, 42: 443-458.

Farouki, O.T., 1981, Thermal Properties of Soils, CRREL Monograph 81-1, Hanover, 151 pp.

Jacobs, P., Sevens, E. and Kunnen, M. 1995, Principles of computerized X-ray tomography and application to building materials, Science of the Total Environment 167 161-170.

Jiang, H., Seco, J. and Paganetti, H. 2007, Effects of Hounsfield number conversion on CT based proton Monte Carlo dose calculations, Medical Physics 34: 1439–1449, DOI: 10,1118/1,2715481.

Leblanc, A.M. 2013. Modélisation tridimensionnelle du régime thermique du pergélisol de la vallée de Salluit au Québec nordique en fonction de différents scénarios de réchauffement climatique. Thèse de doctorat. Québec, Québec, Université Laval, 441 p.

Long, B., DesRoches, M., Mechti, N., Cnuddle, V. and Jacobs, P. 2012, Porosity variations in function of deposit architecture, CT-scan Workshop, Development on non-medical environment, march 2012, 7-9.

Maxwell, J.C. and Thompson, J.J. 1892, A treatise on electricity and magnetism, Vol,1 Clarendon.

Murton, J.B. and French, H.M. 1994, Cryostructures in permafrost, Tuktoyaktuk coastlands, western arctic Canada, Canadian Journal of Earth Sciences 31: 737–747, DOI: 10,1139/e94-067.

Schwerdtfeger, P. 1963, The thermal properties of sea ice, Journal of Glaciology, Vol, 4, No, 36, p, 789- 807.

Slusarchuk, W.A. and Foulger, P.H. 1973, Development and calibration of the thermal conductivity probe apparatus for use in the field and laboratory. National Research Council of Canada, Division of Building Research, NRC 13267. pp.

Slusarchuk, W.A. and Watson, G.H. 1975, Thermal conductivity of some ice-rich permafrost soils, Canadian Geotechnical Journal, 12: 413-423.